

## Three-Dimensional Soundproof Acoustic Metacage

Chenkai Liu<sup>1,2,\*</sup>, Jinjie Shi<sup>1,\*</sup>, Wei Zhao<sup>2,3,\*</sup>, Xiaoxi Zhou,<sup>2</sup> Chu Ma,<sup>4,5</sup> Ruwen Peng<sup>1</sup>, Mu Wang<sup>1</sup>, Zhi Hong Hang,<sup>2,6</sup> Xiaozhou Liu,<sup>1</sup> Johan Christensen<sup>7</sup>, Nicholas X. Fang<sup>5,†</sup> and Yun Lai<sup>1,‡</sup>

<sup>1</sup>MOE Key Laboratory of Modern Acoustics, National Laboratory of Solid State Microstructures, School of Physics, and Collaborative Innovation Center of Advanced Microstructures, Nanjing University, Nanjing 210093, China

<sup>2</sup>School of Physical Science and Technology, Soochow University, Suzhou 215006, China

<sup>3</sup>School of Electronic and Information Engineering, Soochow University, Suzhou 215006, China

<sup>4</sup>Department of Electrical and Computer Engineering, University of Wisconsin–Madison, Madison, Wisconsin 53706, USA

<sup>5</sup>Department of Mechanical Engineering, Massachusetts Institute of Technology,

77 Massachusetts Avenue, Cambridge, Massachusetts 02139, USA

<sup>6</sup>Institute for Advanced Study, Soochow University, Suzhou 215006, China

<sup>7</sup>Department of Physics, Universidad Carlos III de Madrid, ES-28916 Leganes, Madrid, Spain



(Received 14 March 2020; revised 30 September 2020; accepted 26 July 2021; published 16 August 2021)

In this Letter, we theoretically propose and experimentally demonstrate a three-dimensional soundproof acoustic cage structure, hereby denoted as an acoustic metacage. The metacage is composed of six acoustic metamaterial slabs with open holes and hidden bypass space coiling tunnels connected to the holes. Band structure analysis reveals a novel physical mechanism to open a low-frequency broad partial band gap via the band folding in other directions, which can also be interpreted by an effective medium with indefinite effective mass density and negative effective modulus. Transmission loss in simulations and in the acoustic impedance tube are administered. Strikingly, we prove that the soundproofing effect of the metacage is robust against the airflow perturbation induced by a fan. Our work paves a road for low-frequency airborne soundproof structures in the presence of ventilation.

DOI: 10.1103/PhysRevLett.127.084301

Sound insulation is an important issue in acoustics that has applications in various fields like architectural design, urban planning, and transportation. However, the traditional techniques developed to suppress and attenuate sound have some severe limits [1,2]. Phononic crystals [3–5] with acoustic band gaps can block sound efficiently. However, the band gaps of phononic crystals emerge only at high frequencies where the wavelength is comparable to the scale of the microstructure. In the past two decades, acoustic metamaterials [6–8] composed of building blocks in the deep-subwavelength scale have opened a new route for unprecedented artificial acoustic materials. By utilizing acoustic metamaterials [9–12] with low-frequency band gaps, sound insulation has been successfully demonstrated with subwavelength structures [13–19]. Based on acoustic metamaterials, various novel applications have been proposed including negative refraction [20,21], superresolution imaging [22,23], cloaking [24,25], metasurface applications [26,27], exotic elastic properties [28–31], and topological acoustics [32,33], etc. These findings have significantly enhanced the abilities to manipulate acoustic waves.

In practice, a common demand in addition to sound insulation is ventilation, which demands the existence of passages for airflow in the structure design. Interestingly, sound insulation and ventilation can be achieved simultaneously.

Recently, several methods utilizing open-structure metamaterials [15–19,34–37] have been proposed to realize the functionality of simultaneous sound insulation and ventilation. However, these approaches are usually limited to either a narrow working frequency range or a relatively large thickness. Moreover, most of the previous investigations were limited in one or two dimensions. To date, the theoretical design and experimental verification of three-dimensional soundproof open structures are still lacking.

In this Letter, we propose a type of 3D cage structures that can efficiently block sound waves within a low-frequency regime and thus guarantee a “silent” space for airborne sound. The open holes on the cage allow air to access the cage freely in all directions, therefore endowing the function of ventilation. Such a soundproof cage is denoted as an acoustic metacage, shown in Fig. 1(a). The potential applications of 3D acoustic cage structure include a machine room seeking the techniques of sound insulation and heat dissipation, a working room needing sound insulation and fresh air (ventilation contributes to heat dissipation and air flow), and many others.

The physical principle behind the sound insulation phenomenon is related to acoustic labyrinthine metamaterials [12,38,39], which can exhibit extreme constitutive parameters and an exceptional ability to control the phase of sound. Because of the excellent functionalities and ease

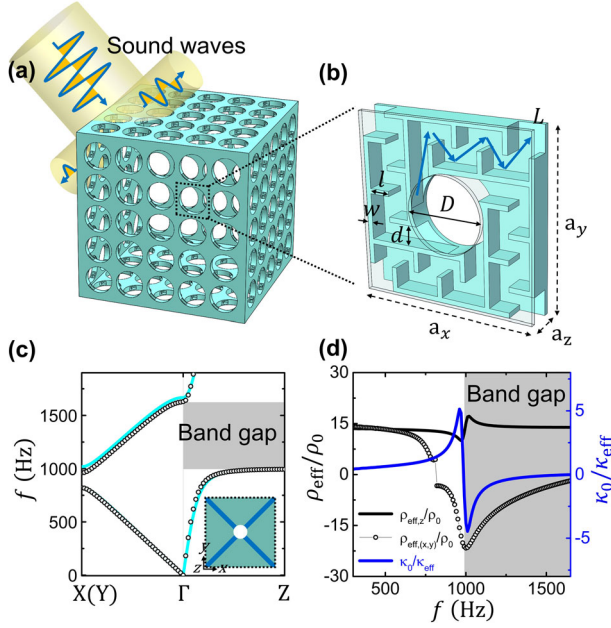


FIG. 1. (a) Schematic diagram of the acoustic metacage with the functionalities of soundproofing and ventilation. (b) Perspective view of the unit cell, composed of a central open hole with a diameter of  $D = 30$  mm and four identical hidden BSCTs with identical geometric parameters of thickness  $w = 2$  mm, length  $l = 8$  mm, and width  $d = 8$  mm that have the overall size of  $a_z = 12$  mm and  $a_x = a_y = a = 70$  mm. The connected blue arrows denote the propagating path for sound waves inside the BSCTs with a total length of  $L \approx 84$  mm, which can be equivalent to a high index  $n$  with straightened tunnels in the simplified view [inset in (c)]. (c) The band structures of the unit cell. The cyan solid lines and black symbol lines are, respectively, obtained from Eq. (1) with  $n = 1.7$ ,  $r = 11.8$ , and full-wave simulation. (d) The normalized effective mass density of  $\rho_{\text{eff},z}/\rho_0$  and  $\rho_{\text{eff},x(y)}/\rho_0$  and effective reciprocal bulk modulus of  $\kappa_0/\kappa_{\text{eff}}$  as a function of the frequency.

of fabrication, labyrinthine metamaterials recently have been extensively applied in the design of acoustic metasurfaces [27] and two-dimensional sound insulation structures [17,19,40]. Here, we find that the combination of labyrinth and anisotropy [41] can lead to a large band gap in the low-frequency regime. The structures are designed as panels with open holes that are connected with bypass space coiling tunnels (BSCTs) hidden in the panels. The unit cell of the metacage is shown in Fig. 1(b). Sound waves now propagate along a straight path in the  $z$  direction and along a zigzag path in the  $xy$  plane. Since the coiled-up space lies perpendicular to the plane of wave propagation, the thickness of such a metacage can be significantly reduced to the deep-subwavelength scale compared to traditional 2D labyrinthine metamaterials.

In order to understand the underlying physics behind the metacage, a physical model has been built to approximately describe the band structures of the unit cell if the tunnels are in a subwavelength scale. The BSCTs are equivalent to

straightened tunnels with an effective high refractive index of  $n$  in the simplified view shown in the inset in Fig. 1(c). By applying the Floquet-Bloch theory, the dispersion relation can be derived and expressed as

$$n \sin(k_0 a_z) \{ \cos(k_y a) + \cos(k_x a) [1 + \cos(k_y a)] - 2 \cos(\sqrt{2} n k_0 a) - 1 \} + r \sin(\sqrt{2} n k_0 a) [ \cos(k_z a_z) - \cos(k_0 a_z) ] = 0, \quad (1)$$

where  $k_{x,y,z}$  and  $k_0$ , respectively, represent the Bloch wave number along the  $x, y, z$  direction and the wave number in the background medium,  $n$  represents the high refractive index in the BSCTs, and  $r$  represents the ratio of cross-sectional area between the hole and the BSCTs connected to the hole. The dispersion relation is solved by Eq. (1), plotted in cyan solid lines in Fig. 1(c). Interestingly, at low frequencies, we observe a partial band gap (gray domain) along the  $\Gamma Z$  direction, indicating the soundproofing properties. At the same frequency range, a negative band along the  $\Gamma X(Y)$  direction is found. Generally, we can describe the bandwidth of the partial band gap as  $f_0 < f < f_1$ , where  $f_0$  is the lower edge, which corresponds to the resonant frequency, while  $f_1$  is the upper edge. The position of the bands can be tuned by  $n$  or the total length of the BSCTs  $L$ , and the bandwidth is related to  $r$ . In this case, the normalized frequencies are set to  $f_0 a_z / c_0 = 0.035$  and  $f_1 a_z / c_0 = 0.057$ , which signifies that the soundproofing effect, in principle, can be realized at a deep-subwavelength scale.

In addition, the band structures of the metamaterial can be numerically obtained by the full-wave simulations (COMSOL Multiphysics), shown in black symbol lines in Fig. 1(c). The mass density and the speed of sound in air are set as  $\rho_0 = 1.21$  kg/m<sup>3</sup> and  $c_0 = 343$  m/s, respectively. The solid frames and hard wall panels are set as rigid in the simulations due to the huge impedance difference between air and the solid materials. For simplification, we neglect the acoustic dissipation here. Except for the little frequency shift resulting from the finite tunnel width, the simulated results agree well with the theory.

In the following, we apply the effective medium theory to analyze the metamaterial [42]. By calculating the complex transmission and reflection coefficients, the retrieved normalized effective mass density and effective reciprocal bulk modulus are depicted in Fig. 1(d). Here,  $\rho_0$  and  $\kappa_0$  denote the mass density and bulk modulus of background medium air, respectively. The demonstration on the validity of the effective medium is shown in Supplemental Material [43]. Because of the resonance induced by the BSCTs,  $\kappa_0/\kappa_{\text{eff}}$  turns negative from about 1000 to 1636 Hz. Meanwhile,  $\rho_{\text{eff},z}/\rho_0$  remains positive, while  $\rho_{\text{eff},x(y)}/\rho_0$  turns negative. Thus, such mass density is indefinite [30,44]. When  $\rho_{\text{eff},z}/\rho_0 > 0$  and  $\kappa_0/\kappa_{\text{eff}} < 0$ , the partial band gap along the  $\Gamma Z$  direction emerges. At the

same frequency regime, sound waves can propagate freely along the  $\Gamma X(Y)$  direction due to the negative band induced by  $\rho_{\text{eff},x(y)}/\rho_0 < 0$  and  $\kappa_0/\kappa_{\text{eff}} < 0$ . Such an observation reveals that the origin and the creation of this partial band gap in the direction of open holes lie in the band folding in other directions. Moreover, hyperbolic dispersions emerge at such a frequency range [45,46] (see Supplemental Material [43]). Such hyperbolic dispersions are also observed in nonlocal acoustic metasurfaces with coupling between neighboring elements which leads to surface waves [47]. Here, we focus on the emergence of large band gaps at the deep-subwavelength limit, which could support a robust soundproofing effect.

To characterize the soundproofing functionality of the unit cell, we have performed the full-wave simulations for transmission. The results of transmission loss (TL) as a function of the frequency with different unit cell numbers are plotted in Fig. 2(a). It is seen that, when  $N = 1$ , the soundproofing phenomenon approximately appears at  $f_0 = 1000$  Hz. We note that the particular wavelength at 1000 Hz ( $\lambda = 343$  mm) is nearly 28.5 times larger than the thickness of the unit cell, i.e.,  $a_z = 12$  mm, confirming that the metamaterial works at the deep-subwavelength scale. Moreover, such a transmission spectrum exhibits the known Fano resonances [17,48], whose peak constitutes an asymmetric profile that is accompanied by a sharp transition between full transmission and full reflection.

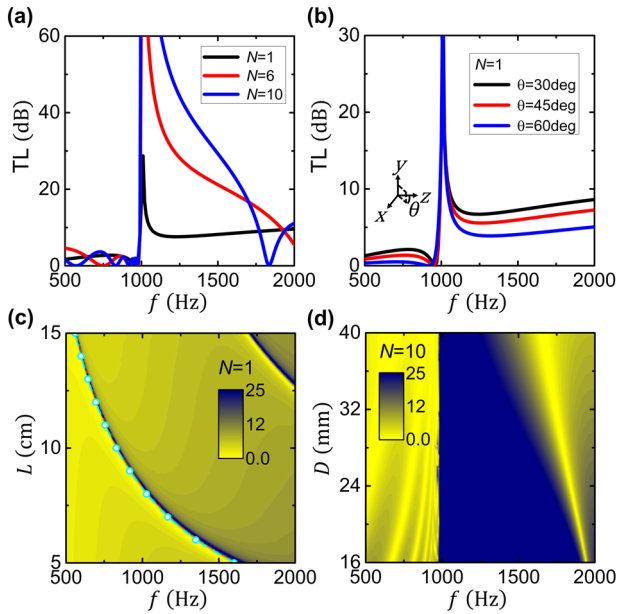


FIG. 2. Simulated TL as a function of the frequency for the unit cell (a) with different unit cell numbers of  $N = 1, 6$ , and  $10$  along the  $z$  direction and (b) with different oblique incident angles of  $\theta = 30^\circ, 45^\circ$ , and  $60^\circ$ . (c) Simulated TL with  $N = 1$  as functions of the frequency and the length of BSCTs. The cyan dotted line represents the theoretical result of the tube resonators with  $S \approx d^2$  ( $d = 8$  mm). (d) Simulated TL with  $N = 10$  as functions of the frequency and the diameter of the central open hole.

When  $N$  increases, the soundproofing bandwidth broadens quickly. For example, the soundproofing bandwidth for 20 dB reaches around 550 Hz when  $N = 6$ . Figure 2(b) shows the results of TL as a function of the frequency at different oblique incident angles, indicating that the soundproofing performance is insensitive to the incident angles.

To quantitatively describe such a partial band gap, the transmission properties on geometrical parameters have been performed, and the results are shown in Figs. 2(c) and 2(d). When one geometric parameter is varying, all the other parameters are fixed. First, we focus on the lower edge of the partial band gap, namely, the resonant frequency  $f_0$ . Figure 2(c) shows the results of TL as functions of the frequency and the total length of the BSCTs. Here, the unit cell number in transmission computation is chosen as  $N = 1$ . We can observe that the dip of the TL is shifted to lower frequency when  $L$  increases. This indicates that  $f_0$  can be tuned toward ultralow frequencies by simply increasing  $L$ . Such a resonant phenomenon has been proved by the theory of tube resonators [49], expressed as  $f_0 \approx c_0/4(L + 0.8\sqrt{S/\pi})$ , where  $c_0$ ,  $S$ , and  $L$  are the speed of sound, the cross-sectional area, and the length of the tubes, respectively. As shown in Fig. 2(c), the theoretical prediction (cyan dotted line) agrees well with the simulated results. We note that four separated resonant frequencies could occur if the BSCTs possess different lengths (see Supplemental Material [43]). Second, we focus on the upper edge of the partial band gap, i.e.,  $f_1$ . We find that  $f_1$  is related to  $r$ , namely, the ratio of cross-sectional area between the hole and the BSCTs located at the connection. For simplification, we adjust only the diameter of the central hole and fix the other geometrical parameters. In order to guarantee sufficient energy decay in the transmission computation, the unit cell number is set as  $N = 10$ . The results of TL as functions of the frequency and the diameter of the central open hole are plotted in Fig. 2(d). It is seen that, when  $D$  decreases, as well as  $r$  decreases,  $f_1$  gradually increases, while  $f_0$  is almost fixed due to a fixed  $L$ . Therefore, the bandwidth of sound insulation increases. From the band structures in Fig. 1(c), we can see that  $f_1$  is determined by the band folding in the  $\Gamma X(Y)$  directions, which is  $2f_0$  in the ideal case. Thus, the fractional bandwidth of the partial band gap, defined as  $(f_1 - f_0)/[(f_1 + f_0)/2]$ , can approach the maximum value of  $2/3$ . This mechanism neatly explains and predicts the broad bandwidth of the band gap, which is beyond the simple picture of Fano resonances.

To experimentally verify the soundproofing effect, we have measured the TL through the unit cell by using an acoustic impedance tube, as shown in Fig. 3(a). A sample of the unit cell is fabricated by stereolithography 3D printing techniques using polylactide, as shown in Fig. 3(b). In the measurements, the sample is closely sandwiched between two parts of the impedance tube. The cross section of the impedance tube is circular with a

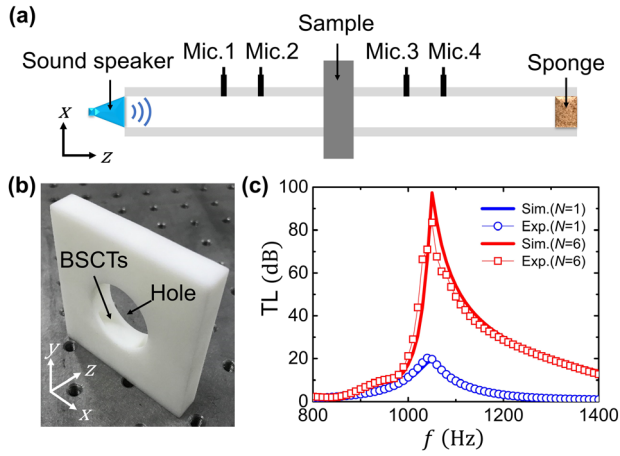


FIG. 3. (a) Diagram of the experimental setup of the impedance tube. (b) Photograph of a real sample fabricated by 3D printing method. (c) Measured and simulated TL as a function of the frequency with different unit cell numbers of  $N = 1$  and 6.

diameter of 30 mm. To prevent sound leakage through the corner holes of the sample, the corner holes are sealed by resin. Thus, the total length of the BSCTs is slightly shorter, and there is a small shift in the resonant frequency. The measured TL as a function of the frequency with different unit cell numbers of  $N = 1, 6$  are shown in Fig. 3(c). For comparison, the simulated results are also plotted. Because of the complexity of loss in practice, the dissipation term can be determined empirically by fitting the measured data. The dissipation term here is chosen as 3.5% loss in the bulk modulus of air in simulations. It is seen that the measured and simulated results match well with each other. Moreover, the soundproofing bandwidth is significantly broadened when  $N = 6$ . The detailed transmittance, reflectance, and absorptance spectrum are shown in Supplemental Material [43]. It is noteworthy that the little loss in practice cannot influence the soundproofing properties discussed before (see Supplemental Material [43]).

Finally, we fabricate a real 3D cage structure to demonstrate the soundproofing properties in the presence of ventilation. The diagram and photography of the experimental setup are shown in Figs. 4(a) and 4(b). The acoustic metacage is constructed by six metamaterial slabs, and each slab consists of  $2 \times 2$  units, as depicted in Fig. 4(b). The sealed unit cell is chosen to construct the 3D metacage in Fig. 3. The whole size is  $164 \text{ mm} \times 164 \text{ mm} \times 164 \text{ mm}$ . A sound speaker (HiVi M4N) is placed head-on to and 50 cm away from the cage. The airflow, including crosswind and tailwind, is produced by a moveable fan (SAB40A) 70 cm away from the cage, and the velocities are measured by hot-wire anemometry (AR866A). A microphone (GRAS 46BE) is mounted on a moving stage to measure the acoustic signals along the scan path [shown as an orange dashed line in Fig. 4(a)] gradually away from the fan in the horizontal plane. The step size of scan path is 5 mm. Sound-absorbing foams are placed around the whole

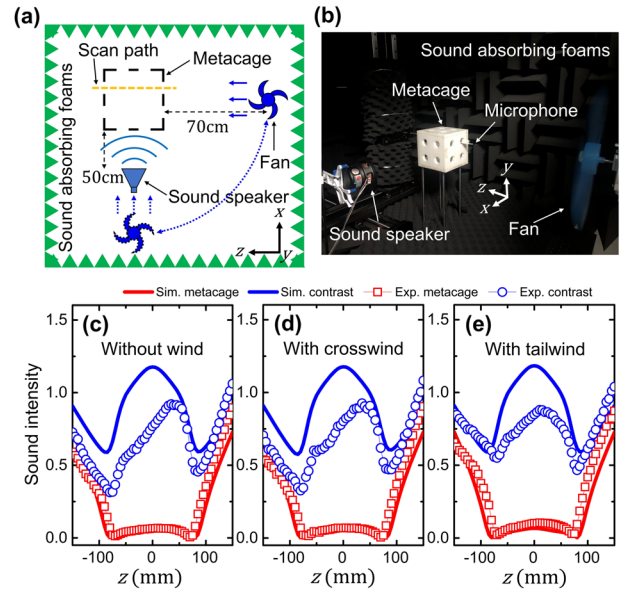


FIG. 4. Experimental demonstration of the soundproofing properties in the presence of ventilation. (a) Diagram and (b) photograph of the experimental setup. (c)–(e) Measured and simulated sound intensity as a function of the measuring position (c) without wind, (d) with crosswind of fan level 1, and (e) with tailwind of fan level 1.

system to reduce the reflection and environmental noise. For comparison, a normal-hole cage (without BSCTs) as a contrast cage is also investigated.

At the working frequency of  $f = 1030 \text{ Hz}$ , the measured and simulated sound intensity as a function of the measuring position are plotted in Figs. 4(c)–4(e), including the cases without wind, with crosswind, and with tailwind. The sound intensity is a normalized quantity defined as  $|p/p_0|^2$ , where  $p$  and  $p_0$  denote the sound pressure (measured in Pa) with and without the cages, respectively. The horizontal axis represents different measuring positions of the microphone scan path, and the origin of coordinates is located at the center of the scan path. The solid and symbol lines, respectively, represent the simulated and measured results. The simulated computation for the case without (with) airflow is based on the pressure acoustics module (aeroacoustics module with linearized potential flow model) of COMSOL Multiphysics.

When there is no airflow in Fig. 4(c), it is seen that the sound intensity is quite large inside the contrast cage. Interestingly, the sound intensity inside the metacage is significantly reduced to a level more than 10 times lower than that of the contrast cage. The measured results (symbol) agree with the simulation (solid lines). Moreover, when some airflow with velocity of 2 m/s is introduced to the system by the nearby fan in Figs. 4(d) and 4(e), the intensity profile remains almost unchanged. The soundproofing performances under a variety of airflow velocities and in different directions are discussed in

Supplemental Material [43]. Such a cage structure with the deep-subwavelength thickness of 12 mm can efficiently create a silent space with a bandwidth of 50 Hz around the working frequency of 1030 Hz (see Supplemental Material [43]). Therefore, such an acoustic metacage can indeed work nicely as a 3D sound shield even with airflow. Moreover, the discussions of different types and positions of sources are also shown in Supplemental Material [43], which demonstrate the robustness of the soundproofing functionality of the metacage under various kinds of sources. Also (see Supplemental Material [43]), we find that the acoustic metacage and the Faraday cage have some properties in common.

In summary, we theoretically and experimentally demonstrate a 3D soundproof acoustic metacage with deep-subwavelength scale. The cage is constructed by strongly anisotropic labyrinthine metamaterials, which leads to broadband negative effective modulus as well as indefinite mass density. A large partial band gap for airborne sound is opened at the low-frequency regime, in accordance with the band folding in other directions. Theoretical, numerical, and experimental results successfully verified our theory. Such low-frequency airborne soundproof structures could have practical benefits in noise control.

Y. L., X. L., M. W., and R. P. acknowledge the financial support from the National Key R&D Program of China (2020YFA0211400, 2020YFA0211300, and 2017YFA0303702), National Natural Science Foundation of China (11974176, 61975078, 11774167, 11634005, and 11974177), and State Key Program of National Natural Science Foundation of China (11834008); J. C. acknowledges the support from the MINECO through a Ramon y Cajal grant (Grant No. RYC-2015-17156) and European Research Council (ERC) through the Starting Grant No. 714577 PHONOMETA. C. M. and N. X. F. acknowledge the support from Exxon Mobil through the MIT Energy Initiative.

\*These authors contributed equally to this work.

†nicfang@mit.edu

‡laiyun@nju.edu.cn

- [1] T. Cox and P. D'Antonio, *Acoustic Absorbers and Diffusers: Theory, Design and Application*, 3rd ed. (CRC Press, Taylor & Francis Group, London, New York, 2017).
- [2] J. F. Allard and N. Atalla, *Propagation of Sound in Porous Media: Modelling Sound Absorbing Materials*, 2nd ed. (Wiley, Hoboken, 2009).
- [3] M. S. Kushwaha, P. Halevi, L. Dobrzynski, and B. Djafari-Rouhani, Acoustic Band Structure of Periodic Elastic Composites, *Phys. Rev. Lett.* **71**, 2022 (1993).
- [4] R. Martínez-Sala, J. Sancho, J. V. Sánchez, V. Gómez, J. Llinares, and F. Meseguer, Sound attenuation by sculpture, *Nature (London)* **378**, 241 (1995).
- [5] F. R. Montero de Espinosa, E. Jiménez, and M. Torres, Ultrasonic Band Gap in a Periodic Two-Dimensional Composite, *Phys. Rev. Lett.* **80**, 1208 (1998).
- [6] G. Ma and P. Sheng, Acoustic metamaterials: From local resonances to broad horizons, *Sci. Adv.* **2**, e1501595 (2016).
- [7] S. A. Cummer, J. Christensen, and A. Alù, Controlling sound with acoustic metamaterials, *Nat. Rev. Mater.* **1**, 16001 (2016).
- [8] H. Ge, M. Yang, C. Ma, M. H. Lu, Y. F. Chen, N. Fang, and P. Sheng, Breaking the barriers: Advances in acoustic functional materials, *Natl. Sci. Rev.* **5**, 159 (2018).
- [9] Z. Liu, X. Zhang, Y. Mao, Y. Y. Zhu, Z. Yang, C. T. Chan, and P. Sheng, Locally resonant sonic materials, *Science* **289**, 1734 (2000).
- [10] N. Fang, D. Xi, J. Xu, M. Ambati, W. Srituravanich, C. Sun, and X. Zhang, Ultrasonic metamaterials with negative modulus, *Nat. Mater.* **5**, 452 (2006).
- [11] Z. Yang, J. Mei, M. Yang, N. H. Chan, and P. Sheng, Membrane-Type Acoustic Metamaterial with Negative Dynamic Mass, *Phys. Rev. Lett.* **101**, 204301 (2008).
- [12] Z. Liang and J. Li, Extreme Acoustic Metamaterial by Coiling up Space, *Phys. Rev. Lett.* **108**, 114301 (2012).
- [13] J. Mei, G. Ma, M. Yang, Z. Yang, W. Wen, and P. Sheng, Dark acoustic metamaterials as super absorbers for low-frequency sound, *Nat. Commun.* **3**, 756 (2012).
- [14] G. Ma, M. Yang, S. Xiao, Z. Yang, and P. Sheng, Acoustic metasurface with hybrid resonances, *Nat. Mater.* **13**, 873 (2014).
- [15] S. H. Kim and S. H. Lee, Air transparent soundproof window, *AIP Adv.* **4**, 117123 (2014).
- [16] J. W. Jung, J. E. Kim, and J. W. Lee, Acoustic metamaterial panel for both fluid passage and broadband soundproofing in the audible frequency range, *Appl. Phys. Lett.* **112**, 041903 (2018).
- [17] R. Ghaffarivardavagh, J. Nikolajczyk, S. Anderson, and X. Zhang, Ultra-open acoustic metamaterial silencer based on Fano-like interference, *Phys. Rev. B* **99**, 024302 (2019).
- [18] G. Ma, M. Yang, Z. Yang, and P. Sheng, Low-frequency narrow-band acoustic filter with large orifice, *Appl. Phys. Lett.* **103**, 011903 (2013).
- [19] Y. Cheng, C. Zhou, B. G. Yuan, D. J. Wu, Q. Wei, and X. J. Liu, Ultra-sparse metasurface for high reflection of low-frequency sound based on artificial mie resonances, *Nat. Mater.* **14**, 1013 (2015).
- [20] S. Zhang, L. Yin, and N. Fang, Focusing Ultrasound with an Acoustic Metamaterial Network, *Phys. Rev. Lett.* **102**, 194301 (2009).
- [21] T. Brunet, A. Merlin, B. Mascaró, K. Zimny, J. Leng, O. Poncelet, C. Aristégui, and O. Mondain-Monval, Soft 3D acoustic metamaterial with negative index, *Nat. Mater.* **14**, 384 (2015).
- [22] J. Li, L. Fok, X. Yin, G. Bartal, and X. Zhang, Experimental demonstration of an acoustic magnifying hyperlens, *Nat. Mater.* **8**, 931 (2009).
- [23] J. Zhu, J. Christensen, J. Jung, L. Martin-Moreno, X. Yin, L. Fok, X. Zhang, and F. J. Garcia-Vidal, A Holey-structured metamaterial for acoustic deep-subwavelength imaging, *Nat. Phys.* **7**, 52 (2011).
- [24] S. Zhang, C. Xia, and N. Fang, Broadband Acoustic Cloak for Ultrasound Waves, *Phys. Rev. Lett.* **106**, 024301 (2011).

- [25] B. I. Popa, L. Zigoneanu, and S. A. Cummer, Experimental Acoustic Ground Cloak in Air, *Phys. Rev. Lett.* **106**, 253901 (2011).
- [26] Y. Xie, W. Wang, H. Chen, A. Konneker, B. I. Popa, and S. A. Cummer, Wavefront modulation and subwavelength diffractive acoustics with an acoustic metasurface, *Nat. Commun.* **5**, 5553 (2014).
- [27] B. Assouar, B. Liang, Y. Wu, Y. Li, J. C. Cheng, and Y. Jing, Acoustic metasurfaces, *Nat. Rev. Mater.* **3**, 460 (2018).
- [28] Y. Lai, Y. Wu, P. Sheng, and Z. Q. Zhang, Hybrid elastic solids, *Nat. Mater.* **10**, 620 (2011).
- [29] Y. Wu, Y. Lai, and Z. Q. Zhang, Elastic Metamaterials with Simultaneously Negative Effective Shear Modulus and Mass Density, *Phys. Rev. Lett.* **107**, 105506 (2011).
- [30] G. Ma, C. Fu, G. Wang, P. Del Hougne, J. Christensen, Y. Lai, and P. Sheng, Polarization bandgaps and fluid-like elasticity in fully solid elastic metamaterials, *Nat. Commun.* **7**, 13536 (2016).
- [31] J. Shi, C. Liu, and Y. Lai, Controlling the effective bending stiffness via out-of-plane rotational resonances in elastic metamaterial thin plates, *New J. Phys.* **20**, 103043 (2018).
- [32] H. He, C. Qiu, L. Ye, X. Cai, X. Fan, M. Ke, F. Zhang, and Z. Liu, Topological negative refraction of surface acoustic waves in a Weyl phononic crystal, *Nature (London)* **560**, 61 (2018).
- [33] X. Zhang, M. Xiao, Y. Cheng, M.-H. Lu, and J. Christensen, Topological sound, *Commun. Phys.* **1**, 97 (2018).
- [34] H. L. Zhang, Y. F. Zhu, B. Liang, J. Yang, J. Yang, and J. C. Cheng, Sound insulation in a hollow pipe with subwavelength thickness, *Sci. Rep.* **7**, 44106 (2017).
- [35] H. L. Zhang, Y. F. Zhu, B. Liang, J. Yang, J. Yang, and J. C. Cheng, Omnidirectional ventilated acoustic barrier, *Appl. Phys. Lett.* **111**, 203502 (2017).
- [36] C. Shen, Y. Xie, J. Li, S. A. Cummer, and Y. Jing, Acoustic metacages for sound shielding with steady air flow, *J. Appl. Phys.* **123**, 124501 (2018).
- [37] Y. Ge, H. X. Sun, S. Q. Yuan, and Y. Lai, Broadband unidirectional and omnidirectional bidirectional acoustic insulation through an open window structure with a metasurface of ultrathin Hooklike meta-atoms, *Appl. Phys. Lett.* **112**, 243502 (2018).
- [38] T. Frenzel, J. David Brehm, T. Bückmann, R. Schittny, M. Kadic, and M. Wegener, Three-dimensional labyrinthine acoustic metamaterials, *Appl. Phys. Lett.* **103**, 061907 (2013).
- [39] S. K. Maurya, A. Pandey, S. Shukla, and S. Saxena, Double negativity in 3D space coiling metamaterials, *Sci. Rep.* **6**, 33683 (2016).
- [40] X. Man, T. Liu, B. Xia, Z. Luo, L. Xie, and J. Liu, Space-coiling fractal metamaterial with multi-bandgaps on subwavelength scale, *J. Sound Vib.* **423**, 322 (2018).
- [41] J. Christensen and F. J. García De Abajo, Anisotropic Metamaterials for Full Control of Acoustic Waves, *Phys. Rev. Lett.* **108**, 124301 (2012).
- [42] V. Fokin, M. Ambati, C. Sun, and X. Zhang, Method for retrieving effective properties of locally resonant acoustic metamaterials, *Phys. Rev. B* **76**, 144302 (2007).
- [43] See Supplemental Material at <http://link.aps.org/supplemental/10.1103/PhysRevLett.127.084301> for detailed discussions of analytical derivation of dispersion relation from Floquet-Bloch theory, validity of effective medium approximation, hyperbolic dispersions induced by indefinite mass density, the case of BSCTs with four different lengths, transmittance, reflectance and absorptance spectrum in a impedance tube, influence of dissipation, the experimental measurements of crosswind and tailwind, bandwidth of the metacage, influence of source position, soundproofing functionality under various kinds of sources, as well as comparison between the metacage and the Faraday cage.
- [44] D. R. Smith and D. Schurig, Electromagnetic Wave Propagation in Media with Indefinite Permittivity and Permeability Tensors, *Phys. Rev. Lett.* **90**, 077405 (2003).
- [45] X. Ao and C. T. Chan, Far-field image magnification for acoustic waves using anisotropic acoustic metamaterials, *Phys. Rev. E* **77**, 025601(R) (2008).
- [46] C. Shen, Y. Xie, N. Sui, W. Wang, S. A. Cummer, and Y. Jing, Broadband Acoustic Hyperbolic Metamaterial, *Phys. Rev. Lett.* **115**, 254301 (2015).
- [47] L. Quan and A. Alù, Hyperbolic Sound Propagation over Nonlocal Acoustic Metasurfaces, *Phys. Rev. Lett.* **123**, 244303 (2019).
- [48] A. E. Miroshnichenko, S. Flach, and Y. S. Kivshar, Fano resonances in nanoscale structures, *Rev. Mod. Phys.* **82**, 2257 (2010).
- [49] V. M. García-Chocano, R. Graciá-Salgado, D. Torrent, F. Cervera, and J. Sánchez-Dehesa, Quasi-two-dimensional acoustic metamaterial with negative bulk modulus, *Phys. Rev. B* **85**, 184102 (2012).